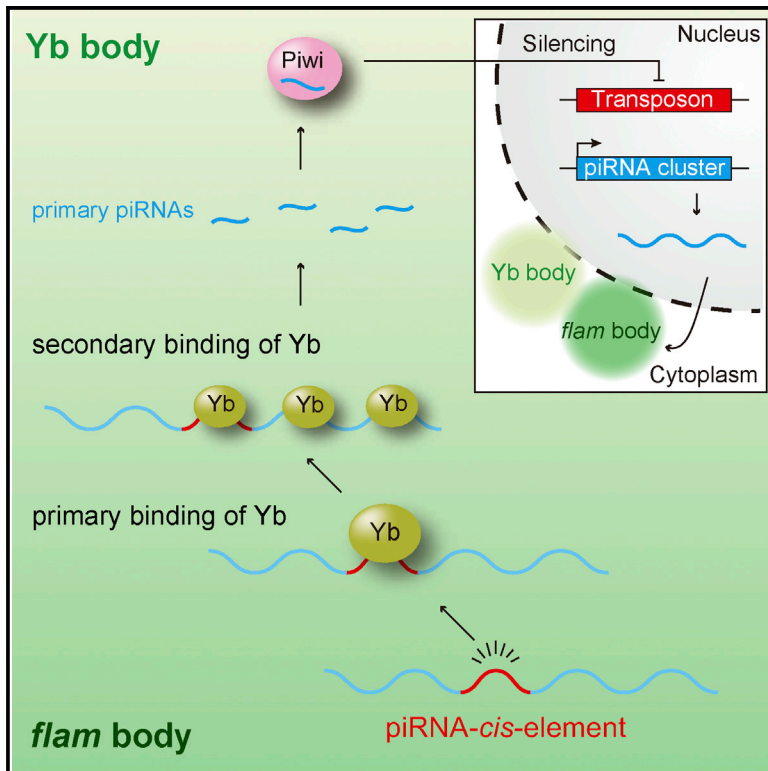


Somatic Primary piRNA Biogenesis Driven by *cis*-Acting RNA Elements and *trans*-Acting Yb

Graphical Abstract



Authors

Hirotsugu Ishizu, Yuka W. Iwasaki, Shigeki Hirakata, ..., Wataru Iwasaki, Haruhiko Siomi, Mikiko C. Siomi

Correspondence

siomim@bs.s.u-tokyo.ac.jp

In Brief

piRNAs protect the germline genome from transposons, although the underlying mechanism remains elusive. Ishizu et al. focused on understanding how piRNA sources are selectively determined from all cellular RNAs. They successfully identified the particular RNA elements necessary and sufficient for producing piRNAs and determined Yb protein as the *trans*-acting partner.

Highlights

- *cis* elements for producing somatic primary piRNAs were identified
- Yb primary binding to *cis* elements in piRNA precursors initiates piRNA production
- Yb secondary binding downstream of *cis* elements does not initiate piRNA production
- Artificial piRNAs from the Yb-*cis*-element system elicit transcriptional silencing

Accession Numbers

GSE69625



Somatic Primary piRNA Biogenesis Driven by *cis*-Acting RNA Elements and *trans*-Acting Yb

Hirotsugu Ishizu,¹ Yuka W. Iwasaki,² Shigeki Hirakata,¹ Haruka Ozaki,³ Wataru Iwasaki,^{1,3} Haruhiko Siomi,² and Mikiko C. Siomi^{1,*}

¹Department of Biological Sciences, Graduate School of Science, The University of Tokyo, Tokyo 113-0032, Japan

²Department of Molecular Biology, Keio University School of Medicine, Tokyo 160-8582, Japan

³Department of Computational Biology, Graduate School of Frontier Sciences, The University of Tokyo, Tokyo 113-0032, Japan

*Correspondence: siomim@bs.s.u-tokyo.ac.jp

<http://dx.doi.org/10.1016/j.celrep.2015.06.035>

This is an open access article under the CC BY-NC-ND license (<http://creativecommons.org/licenses/by-nc-nd/4.0/>).

SUMMARY

Primary piRNAs in *Drosophila* ovarian somatic cells arise from piRNA cluster transcripts and the 3' UTRs of a subset of mRNAs, including *Traffic jam* (*Tj*) mRNA. However, it is unclear how these RNAs are determined as primary piRNA sources. Here, we identify a *cis*-acting 100-nt fragment in the *Tj* 3' UTR that is sufficient for producing artificial piRNAs from unintegrated DNA. These artificial piRNAs were effective in endogenous gene transcriptional silencing. Yb, a core component of primary piRNA biogenesis center Yb bodies, directly bound the *Tj*-*cis* element. Disruption of this interaction markedly reduced piRNA production. Thus, Yb is the *trans*-acting partner of the *Tj*-*cis* element. Yb-CLIP revealed that Yb binding correlated with somatic piRNA production but *Tj*-*cis* element downstream sequences produced few artificial piRNAs. We thus propose that Yb determines primary piRNA sources through two modes of action: primary binding to *cis* elements to specify substrates and secondary binding to downstream regions to increase diversity in piRNA populations.

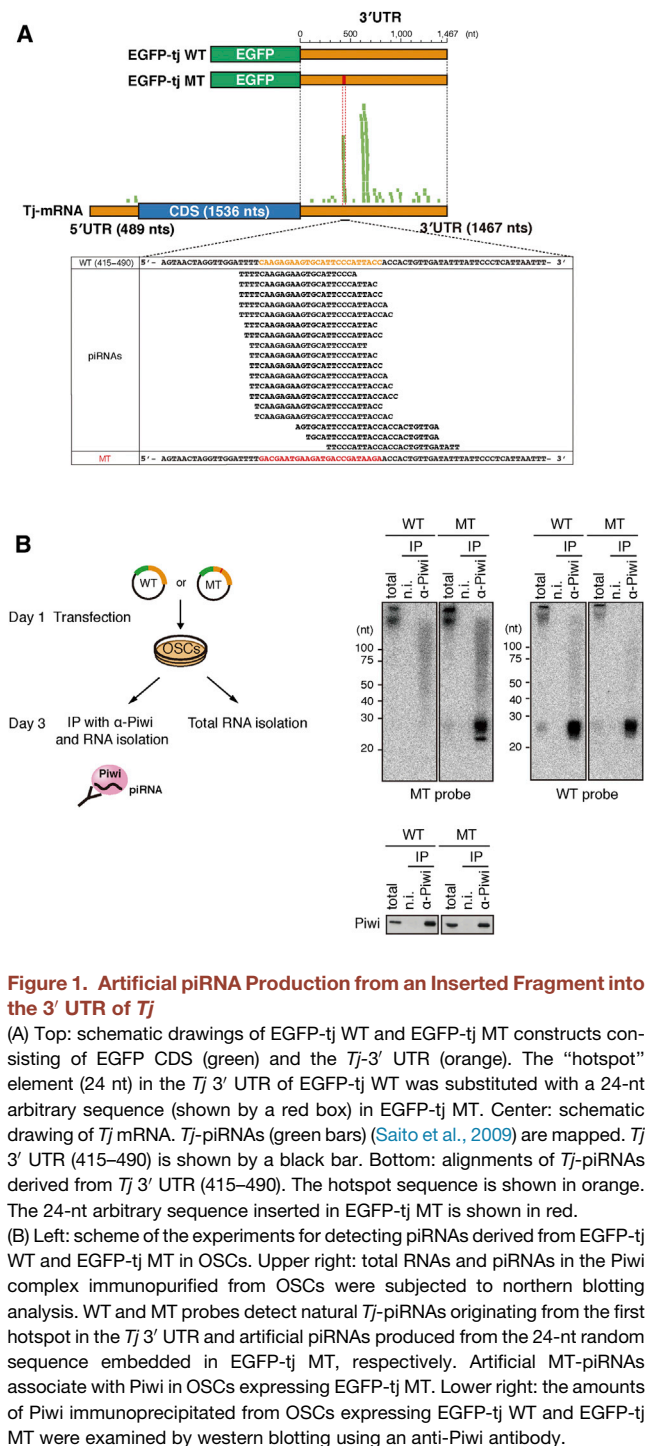
INTRODUCTION

PIWI-interacting RNAs (piRNAs) interact with PIWI proteins to form piRNA-induced silencing complexes (piRISCs), which repress target genes, mostly transposons, either transcriptionally or at the post-transcriptional level by cleaving transcripts in the cytoplasm (Aravin et al., 2007; Brennecke et al., 2007; Ghildiyal and Zamore, 2009; Ishizu et al., 2012; Juliano et al., 2011; Khurana and Theurkauf, 2010; Siomi et al., 2011). Interestingly, not all cells in the gonads use both mechanisms. Follicle cells in *Drosophila* ovaries use transcriptional silencing but lack piRISC-mediated post-transcriptional silencing, while germ cells possess both transcriptional and post-transcriptional piRISC machineries (Ishizu et al., 2012). In *Bombyx* ovaries, only post-transcriptional silencing occurs (Kawaoka et al., 2009). This variation largely depends on which PIWI proteins are expressed in a

given cell type; transcriptional silencing requires nuclear PIWI proteins while post-transcriptional silencing requires cytoplasmic PIWI proteins (Huang et al., 2013; Malone et al., 2009).

Primary piRNAs are produced from single-stranded long non-coding RNAs transcribed from piRNA clusters in a Dicer-independent manner (Houwing et al., 2007; Vagin et al., 2006). The *Drosophila* genome contains 142 piRNA clusters (Brennecke et al., 2007), whose expression is regulated differently in different cell types. *flamenco* (*flam*), a representative of unidirectional piRNA clusters, is expressed only in follicle cells, whereas the bidirectional cluster *42AB* is expressed specifically in nurse cells (Brennecke et al., 2007). The types of transposon fragments inserted in individual piRNA clusters also vary; therefore, piRNA populations differ among cell types. piRNAs in nurse cells are rather complex because primary piRNAs are amplified through the amplification loop, yielding secondary piRNAs (Ishizu et al., 2012). Recent studies showed that secondary piRNAs further produce phased trailer piRNAs (Han et al., 2015; Mohn et al., 2015). Follicle cells do not use this amplification system and thus only contain primary piRNAs.

The biogenesis of somatic primary piRNAs has been studied using ovaries and an ovarian somatic cell (OSC) line (Olivieri et al., 2010; Saito et al., 2009). A current model suggests that upon transcription *flam*-piRNA precursors are localized to perinuclear Flam bodies (Murota et al., 2014) and processed at adjacent Yb bodies (Olivieri et al., 2010; Saito et al., 2010). Yb bodies contain many piRNA factors besides Yb (Haase et al., 2010; Olivieri et al., 2012; Qi et al., 2011; Saito et al., 2009; Saito et al., 2010; Zamparini et al., 2011). Zucchini (Zuc), an endonuclease required for processing piRNA intermediates into mature piRNAs, is localized on the surface of mitochondria (Choi et al., 2006; Han et al., 2015; Ipsaro et al., 2012; Mohn et al., 2015; Nishimasu et al., 2012; Olivieri et al., 2012). Yb bodies tend to be observed in inter-mitochondrial regions (Murota et al., 2014; Nishimasu et al., 2012; Szakmary et al., 2009). This arrangement of organelles appears crucial for accelerating piRNA processing because it centralizes all the necessary factors in the cytoplasm. Upon maturation, piRNAs associate with Piwi, a *Drosophila* PIWI protein, to form piRISCs, which are then translocated to the nucleus to implement nuclear transposon silencing through chromatin modifications on target transposon loci with support from co-factors such as GTSF1/Asterix and Maelstrom (Dönertas et al., 2013; Ishizu et al.,



2012; Muerdter et al., 2013; Ohtani et al., 2013; Olivieri et al., 2010; Saito et al., 2010)

flam is the major source of primary piRNAs in OSCs and follicle cells in the ovaries (Brennecke et al., 2007; Malone et al., 2009; Saito et al., 2009). *flam* is largely occupied by transposon remnants, whose orientation predominantly opposes that of the parental transposons; thus, most primary piRNAs arising from

the piRNA cluster act as antisense oligos to repress parental transposons (Brennecke et al., 2007; Malone et al., 2009; Saito et al., 2009). Some protein-coding genes such as *Traffic jam* (*Tj*) also act as primary piRNA sources (Robine et al., 2009; Saito et al., 2009), and genic piRNA sources express proteins in OSCs and follicle cells. The TJ protein, encoded by *Tj*, is a large Maf transcriptional factor necessary for controlling gonad morphogenesis (Li et al., 2003). Loss of *Tj* function abolishes Piwi expression in follicle cells. However, Piwi expression in nurse cells is not influenced by TJ loss. Thus, the dependence of Piwi expression on TJ differs between follicle cells and germ cells (Saito et al., 2009).

Only a limited number of transcripts serve as somatic primary piRNA precursors. However, the mechanism underlying the recognition and selection of these transcripts as piRNA precursors is poorly understood. To better understand the mechanism, we used the *Tj* 3' UTR as representative of somatic primary piRNA sources to identify a *cis* element and its *trans*-acting partner necessary for producing primary piRNAs in OSCs.

RESULTS

Production of Artificial Primary piRNAs from a Random Sequence Inserted into the *Tj* 3' UTR

First, we constructed a plasmid, EGFP-tj WT, consisting of the EGFP coding sequence (CDS; 717 nt) and the *Tj* 3' UTR (1,467 nt) (Figure 1A). We previously showed that piRNAs are not produced uniformly along the *Tj* 3' UTR; rather, it contains two hotspots that generate substantial amounts of *Tj*-piRNAs (Saito et al., 2009). In the current study, the first hotspot (24 nt) in EGFP-tj WT was replaced with a 24-nt arbitrary sequence, yielding a mutant construct, EGFP-tj MT (Figure 1A). The 24-nt sequence did not match any region in the *Drosophila* genome (data not shown).

OSCs were transfected individually with EGFP-tj WT and EGFP-tj MT constructs. After transfection, northern blotting was performed with two specific probes, WT and MT, designed to detect natural *Tj*-piRNAs originating from the first hotspot in the *Tj* 3' UTR and artificial piRNAs produced from the 24-nt random sequence embedded in EGFP-tj MT, respectively. The MT probe detected small RNAs of 23–29 nt in length among total RNAs isolated from OSCs after transfection with EGFP-tj MT (Figure 1B). Interestingly, the signals were highly enriched in the Piwi-piRISC fraction immunopurified from OSCs, demonstrating that the artificial piRNAs produced from the 24-nt random sequence in EGFP-tj MT were loaded onto Piwi (Figure 1B). These artificial piRNAs (MT-piRNAs) were undetected in OSCs transfected with EGFP-tj WT, confirming MT probe specificity (Figure 1B). The WT probe detected *Tj*-piRNAs in both cells (Figure 1B). However, the signal intensity appeared slightly higher in OSCs transfected with EGFP-tj WT, likely because of exogenous expression of *Tj*-piRNAs from the construct.

Identification of a *cis*-Acting Element in the *Tj* 3' UTR

To narrow down the region that acts as a *cis* element in the expression of MT-piRNAs from EGFP-tj MT, three deletion mutants, MT-1 to MT-3, were produced (Figure 2A). A control

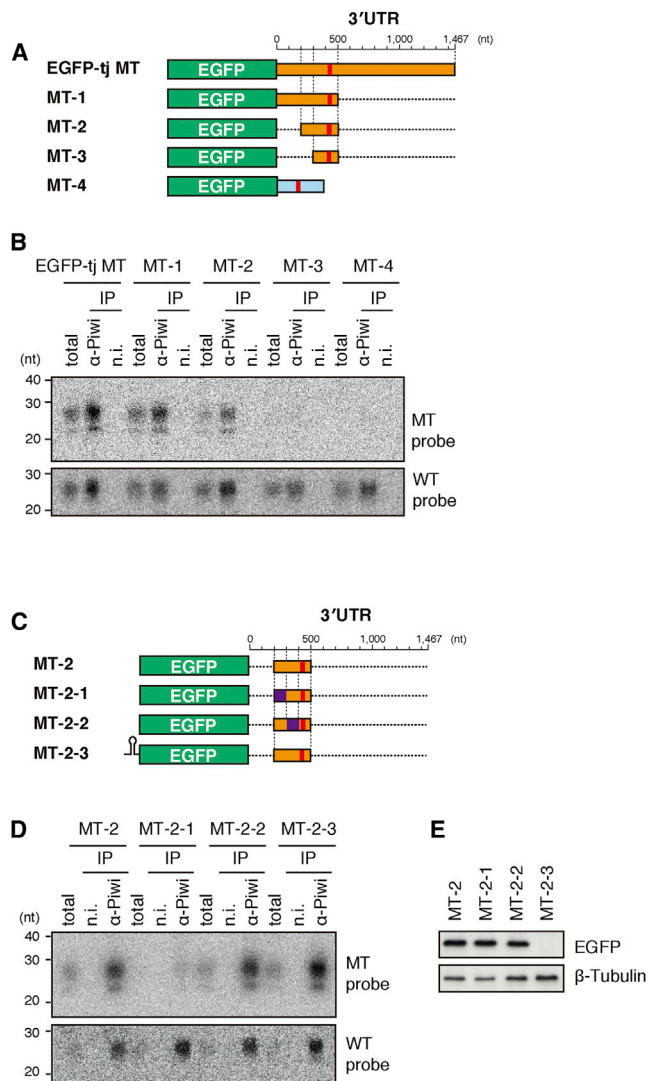


Figure 2. Identification of a cis-Regulatory Element in the *Tj* 3' UTR
 (A) Schematic drawings of EGFP-tj MT and its mutant constructs. MT-4 contains the *Actin42A* 3' UTR (360 nt) (light blue) instead of the *Tj* 3' UTR. The 24-nt artificial sequence (red) exists also in MT-4.
 (B) WT-piRNA and MT-piRNA production was monitored by northern blotting analysis using WT and MT probes as in Figure 1B.
 (C) Schematic drawings of MT-2 and its mutant constructs. The 100-nt random sequence inserted in MT-2-1 and MT-2-2 is shown (purple). A stable stem-loop structure was inserted into the 5' UTR of MT-2-3 to inhibit EGFP translation.
 (D) WT-piRNA and MT-piRNA production was monitored by northern blotting analysis using WT and MT probes as in Figure 2B.
 (E) Western blotting shows the expression levels of EGFP protein in OSCs after transfection. β-tubulin was detected as a loading control.

construct, MT-4, in which the *Tj* 3' UTR was substituted with the *Actin42A* 3' UTR, was also produced (Figure 2A). The 24-nt insertion was maintained in the *Actin42A* 3' UTR of MT-4.

Total RNAs isolated from OSCs and RNAs from the Piwi-piRISC fraction immunopurified from cells were subjected to northern blotting. MT-piRNAs were produced to a similar extent

from MT-1 and MT-2 as from EGFP-tj MT (Figure 2B). In sharp contrast, MT-3 and MT-4 failed to produce MT-piRNAs (Figure 2B). MT-3 and MT-4 mRNA expression levels were nearly equal to those of MT-1 and MT-2 (Figure S1A), suggesting that the 100-nt fragment present in MT-2 but missing from MT-3 serves as the *cis* element for producing MT-piRNAs from downstream regions.

To confirm that the 100-nt fragment acts as a bona fide *cis*-acting element for generating MT-piRNAs, the element was replaced with a 100-nt random sequence, yielding MT-2-1 (Figure 2C). Another mutant, MT-2-2, was produced by exchanging the second 100-nt region of the 3' UTR in MT-2 with the random sequence inserted into MT-2-1 (Figure 2C). Northern blotting revealed that MT-2-2, but not MT-2-1, expressed MT-piRNAs similarly to MT-2 (Figure 2D).

Tj encodes *Tj*-piRNAs and *Tj* protein, both of which are detected in OSCs and ovaries (Brennecke et al., 2007; Li et al., 2003; Malone et al., 2009; Saito et al., 2009). We next assessed if MT-2 mRNA translation is required for primary piRNA production. A hairpin structure that would presumably interfere with translation was inserted into the 5' UTR of MT-2, yielding MT-2-3 (Figure 2C). Western blotting using an anti-EGFP antibody confirmed that no EGFP was expressed from MT-2-3 (Figure 2E). MT-2-3 mRNAs were expressed in OSCs (Figure S1B). Likewise, MT-piRNAs were expressed from MT-2-3 to a similar extent as from MT-2 and MT-2-2 (Figure 2D). Thus, translation of piRNA precursors appears to be dispensable for primary piRNA production.

Deletion of the *Tj*-*cis* Element from the *Drosophila* Genome using the CRISPR/Cas9 System

To examine whether deletion of the *Tj*-*cis* element from the *Drosophila* genome would cause defective *Tj*-piRNA biogenesis, we used the CRISPR/Cas9 system (Hsu et al., 2014). We constructed three plasmids expressing short-guide RNAs (sgRNAs) that target specific sites in the *Tj* locus: targets 1–3 (Figure 3A). sgRNAs were expressed in OSCs for targeting either target 1 + target 2 or target 1 + target 3. We then performed PCR to examine if genomic deletion occurred as expected. DNA fragments of the expected sizes, 599 nt (target 1 + target 2) and 530 nt (target 1 + target 3), were detected only when sgRNAs had been expressed (Figure S2A). Single PCR bands were produced after cloning of each cell line (Figure 3A). Sequencing of the PCR fragments determined the purity of the clones and the deletion sites (Figure S2B), confirming the generation of two deletion mutant cell lines: OSC-Δ*tj*-*cis* 1 and OSC-Δ*tj*-*cis* 2.

We conducted northern blotting using a WT probe (Figure 1B) to detect endogenous *Tj*-piRNAs in both wild-type and mutant OSC lines. This revealed that the piRNAs arising from the first *Tj* 3' UTR hotspot (Figure 1A) in normal OSCs were barely detected in OSC-Δ*tj*-*cis* 1 and OSC-Δ*tj*-*cis* 2 cells (Figure 3B). The production of *Idexis*-piRNAs arising from other genomic loci was barely affected by *Tj*-*cis*-element deletion (Figure 3B). Deep sequencing and genome mapping of piRNAs co-immunoprecipitated with Piwi showed that the numbers of *Tj*-piRNAs, particularly from the 200-nt region neighboring the *Tj*-*cis* element, were severely decreased in OSC-Δ*tj*-*cis* 1 and

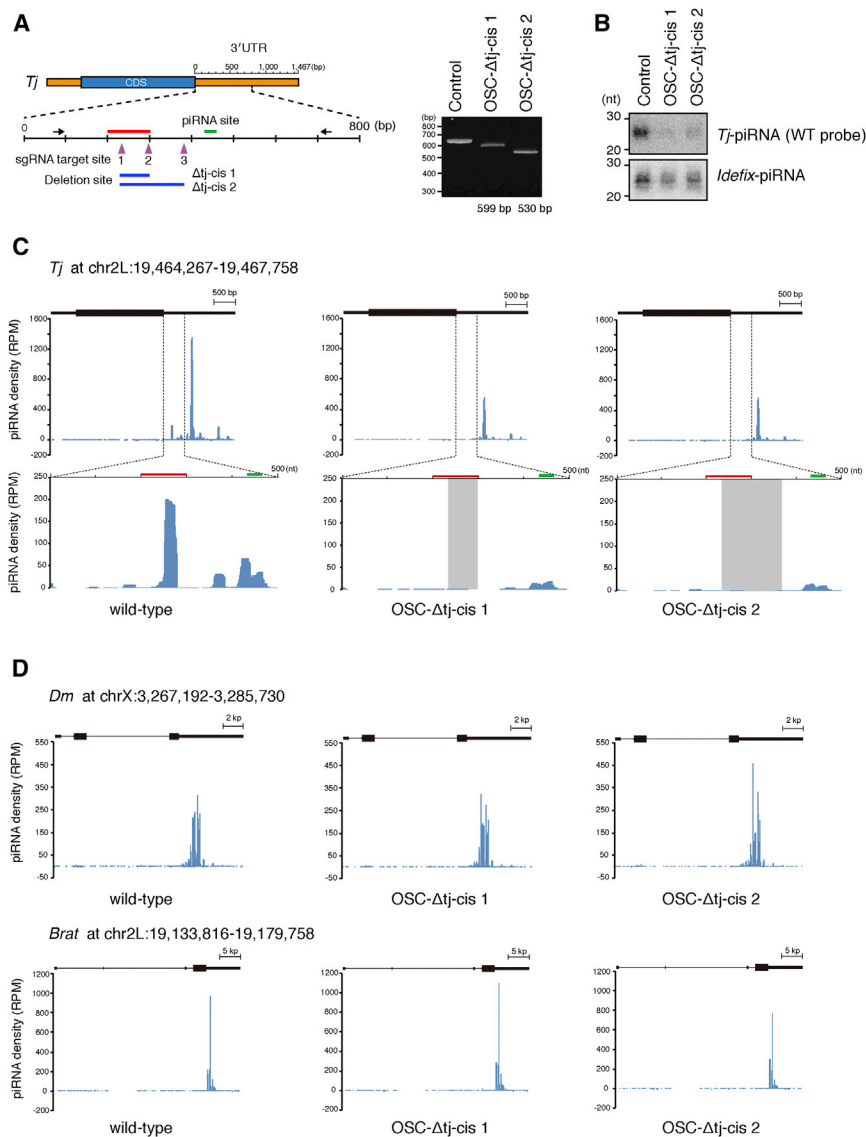


Figure 3. Deletion of the *Tj-cis* Element by CRISPR/Cas9 from the *Drosophila* Genome

(A) Targeting sites of three sgRNAs, sgRNA1, sgRNA2, and sgRNA3 are shown by purple triangles. Genomic regions deleted from the *Tj* locus by CRISPR/Cas9 system are shown by blue bars. Green bar represents the hotspot in the *Tj* 3' UTR. The 599- and 530-nt PCR bands in Figure S2A became single after cloning of the cell lines OSC- Δ *tj-cis* 1 and OSC- Δ *tj-cis* 2, respectively.

(B) Northern blotting was performed on total RNAs isolated from OSC- Δ *tj-cis* 1 and OSC- Δ *tj-cis* 2 using the WT probe. *Idefix*-piRNA was detected as a control.

(C) Distribution of *Tj*-piRNAs. Signals are displayed as reads per million (RPM) values. The lower panels show enlarged views of the *Tj* 3' UTR (1–500). Red and green lines represent the *Tj-cis* element and the hotspot, respectively. Gray boxes show deletion sites.

(D) Distribution of genic piRNAs derived from *Dm* and *Brat*.

OSC- Δ *tj-cis* 2 cells (Figure 3C), piRNAs corresponding to the deletion sites were no longer detected, confirming deletion of the genomic elements. piRNAs mapped to the *Tj* 3' UTR showed little difference between OSC- Δ *tj-cis* 1 and OSC- Δ *tj-cis* 2, agreeing with the observation that MT-3 failed to produce MT-piRNAs (Figure 2B). *Dm* and *Brat* 3' UTRs are known as genic piRNA sources (Saito et al., 2009) and the levels of *Dm*-piRNAs and *Brat*-piRNAs originating from them were unaffected in both mutant cell lines (Figure 3D). These results suggest that the *Tj-cis* element identified in this study acts as a *cis*-regulatory element for producing endogenous *Tj*-piRNAs from the neighboring region in OSCs.

The *Tj-cis* Element Is Sufficient for Producing piRNAs from Downstream Regions

To determine whether the *Tj-cis* element is sufficient for producing piRNAs from unintegrated DNA, we constructed

plasmid EGFP-*tj-cis*, consisting of the EGFP CDS, the *Tj-cis* element, and four tandem repeats of a 25-nt fragment from which artificial piRNAs were designed to be exogenously expressed (Figure 4A). We confirmed that the sequence was not found in the *Drosophila* genome (data not shown). Another mutant, MT-5, was also constructed, in which the *Tj-cis* element and tandem repeat positions in EGFP-*tj-cis* were swapped (Figure 4A). Northern blotting showed that in sharp contrast to EGFP-*tj-cis*, MT-5 expressed few piRNAs from the tandem repeats (Figure 4B). The expression levels of the two constructs were similar (Figure S3). These results verify that the *Tj-cis* element is sufficient to express artificial piRNAs from downstream, but not upstream, arbitrary elements.

We then deep-sequenced primary piRNAs associated with Piwi in OSCs expressing EGFP-*tj-cis* and mapped them on the construct. This revealed that piRNAs can be generated throughout the 3' UTR, not only from the random sequence consisting of four identical repeats, but also from the *Tj-cis* element and polylinker regions (Figure 4C). Both endogenous and exogenous piRNAs mapped to the *Tj-cis* element, and only a few sequence reads corresponding to the EGFP CDS were detected. These results corroborate that the *Tj-cis* element expressed piRNAs from downstream, but hardly at all from upstream elements. It also agrees with the observation that a limited number of piRNAs mapped upstream of the *Tj-cis* element, including the *Tj* CDS and *Tj* 5' UTR (Robine et al., 2009). Characteristics of the artificial piRNAs derived from the EGFP-*tj-cis* construct are summarized (Figures 4D–4F).

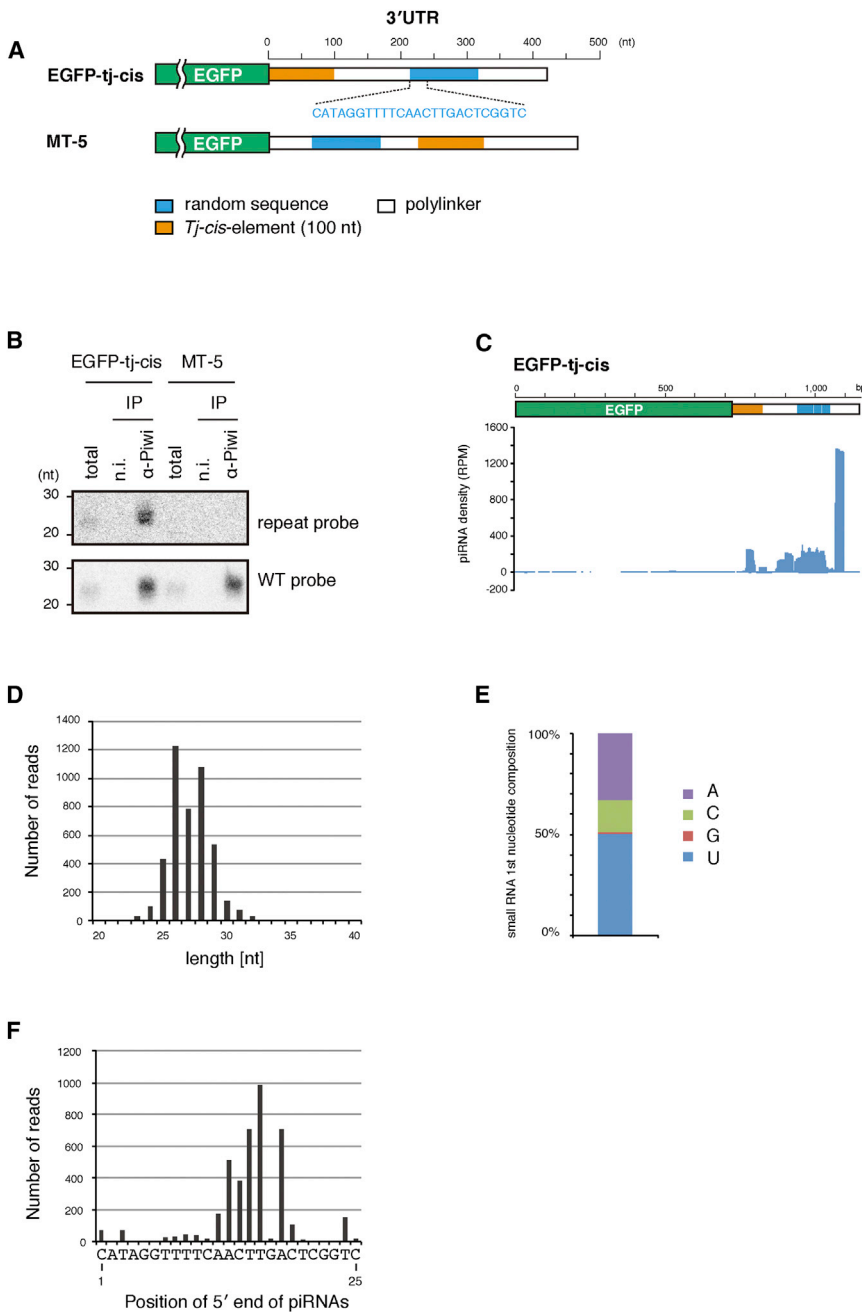


Figure 4. The *Tj-cis* Element Is Sufficient to Produce Genic piRNAs from Its Downstream Region

(A) Schematic drawings of EGFP-tj-cis and its mutant constructs. The *Tj-cis* element (100 nt) is shown in orange. Blue boxes indicate 25-nt random sequences, which are repeated four times in each construct.

(B) Artificial piRNAs derived from the random sequences [blue in (A)] were detected by northern blotting using a 50-nt probe complementary to two tandem repeats. The WT probe detected endogenous *Tj*-piRNAs.

(C) piRNA sequencing reads mapping to the EGFP-tj-cis construct. Signals are displayed as RPM values.

(D) The size distribution of piRNAs derived from the repeat region in EGFP-tj-cis.

(E) Bar diagrams indicating nucleotide of 5' end in piRNAs mapped to the repeat region.

(F) piRNA 5' end coverage over a 25-nt random sequence (minimal unit of the repeat sequence).

Yb-CLIP mapping data with piRNA mapping data obtained in this study (Figure 3C; wild-type) showed that they greatly overlap (Figure S4C), suggesting the direct involvement of Yb in determining substrates in somatic primary piRNA biogenesis.

Unlike MT-2, MT-3 failed to produce artificial MT-piRNAs in OSCs (Figures 2A and 2B). However, Yb-binding marks were observed on regions shared with MT-2 and MT-3 (Figures 2A and 5A). *Tj-R1*, a 121-nt sequence adjacent to the *Tj-cis* element, was within the shared regions, so we next investigated whether *Tj-R1* could also produce artificial piRNAs. The *Tj-cis* element in EGFP-tj-cis (Figure 4A) was replaced with *Tj-R1* to yield construct MT-6 (Figure 5B). Northern blotting revealed that limited artificial piRNAs were produced from MT-6 in sharp contrast to EGFP-Tj-cis (Figures 5B and S4D). RNA immunoprecipitation (RIP) experiments followed by qRT-PCR showed that MT-6 transcripts

only weakly bound Yb (Figure 5C). This suggested that despite the close proximity of *Tj-R1* to the *Tj-cis* element and Yb-binding marks determined by CLIP, it was ineffective in driving piRNA production. We also constructed MT-7, in which *Tj-R1* was replaced with *Tj-R2*, encompassing another 100-nt sequence following *Tj-R1*. MT-7 transcripts showed little Yb-binding capacity and produced only a small amount of artificial piRNAs (Figures 5B, 5C, and S4D). Yb-RNA binding determined by CLIP may therefore reflect primary binding to *cis* elements that provokes piRNA production, and secondary binding that does not provoke piRNA production but determines the domains to

Primary piRNA Production Largely Depends on Yb Binding to the *cis* element

We previously performed HITS crosslinking immunoprecipitation (CLIP) experiments in OSCs using an anti-Yb antibody (Murota et al., 2014). Here, to expand the read numbers, we constructed two new Yb-CLIP libraries (Figure S4A), which showed a high correlation for tag sequences (Figure S4B). Bioinformatic analysis revealed that Yb bound strongly and persistently with the *Tj* 3' UTR, but not the *Tj* CDS or 5' UTR (Figure 5A). The *Tj-cis* element resided in one of the strong, if not the strongest, Yb association sites in the 3' UTR (Figure 5A). Comparison of

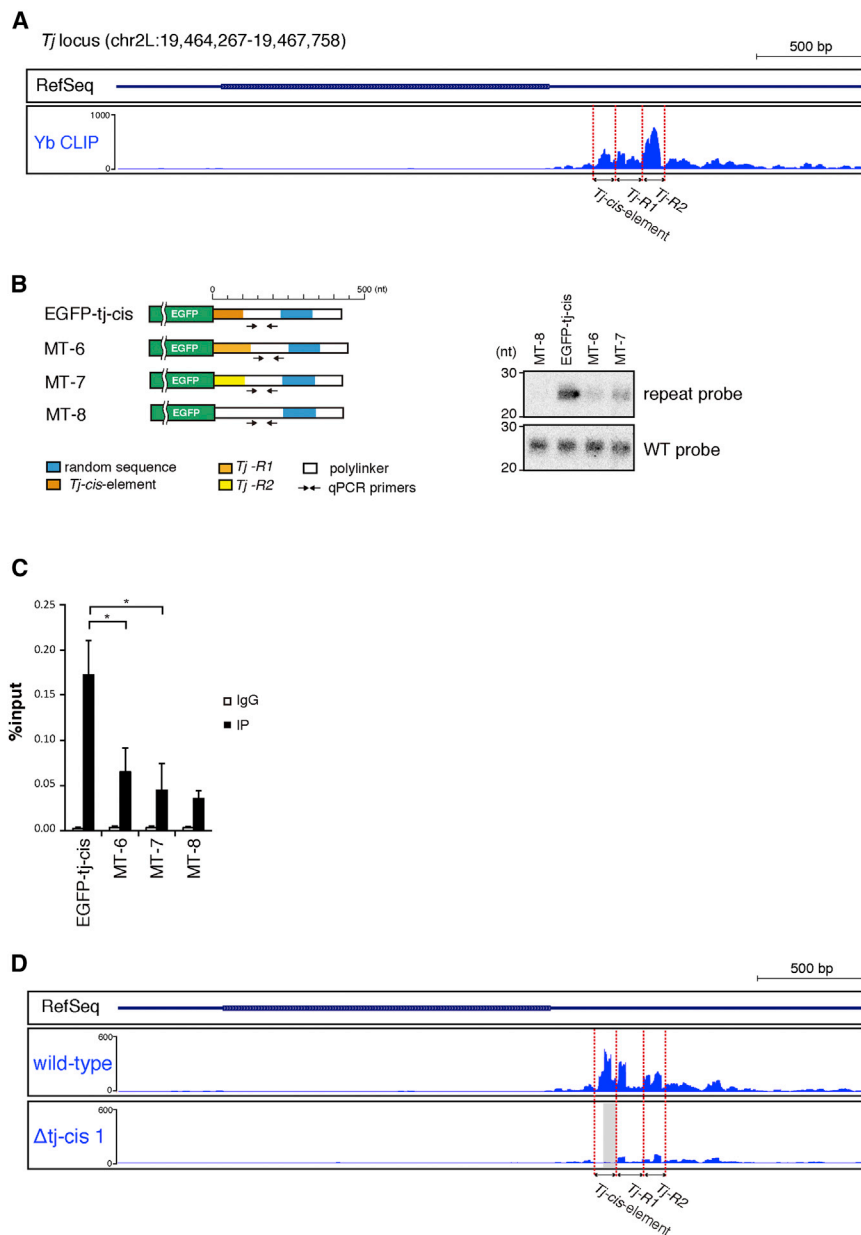


Figure 5. The *Tj-cis* Element, but Not *Tj-R1* and *Tj-R2*, Triggers Artificial piRNA Production

(A) A browser view of Yb-CLIP tags mapped onto the *Tj* locus. Signals are displayed as read counts. (B) Schematic of EGFP-*tj-cis*, MT-6, MT-7, and MT-8. Northern blotting was performed as in Figure 4B.

(C) RIP-qPCR analysis shows that transcripts from MT-6, MT-7, and MT-8 only weakly bound Yb in OSCs. The primers used for qPCR are indicated by arrows in (B). Bars represent means \pm SD of three independent experiments (* $p < 0.05$).

(D) Yb-CLIP mapping data show that Yb binding of the *Tj-R1* and *Tj-R2* regions in the *Drosophila* genome is low in OSC- $\Delta tj-cis1$ (Figure 3A). Signals are displayed in RPM.

be processed in piRNA production. HITS-CLIP experiments using OSC- $\Delta tj-cis 1$ (Figure 3A) revealed that when the *Tj-cis* element was deleted from the *Drosophila* genome, Yb only slightly bound the *Tj-R1* and *Tj-R2* regions within the genome (Figure 5D). These results agree with the observation that MT-6 and MT-7 produced a limited amount of piRNAs (Figure 5B) and further support our original idea that Yb binding to *Tj-R1* and *Tj-R2* shown by Yb-CLIP (Figure 5A) is a secondary event depending on the primary binding of Yb to the *Tj-cis* element.

We enumerated 57,079 Yb-binding positions by identifying crosslinking-induced mutation sites (CIMSs) (Zhang and Darnell, 2011), which clarified that the nucleotide composition around CIMSs showed strong U peaks (Figure S4E). Although

UV crosslinking has been shown to occur preferentially at U-rich stretches (Sugimoto et al., 2012), it does not exclude the possibility that Yb shows a U bias in its RNA binding. CIMSs were found in the *Tj-cis* element, *Tj-R1*, and *Tj-R2* (Figure S4F), suggesting that it would be difficult to distinguish primary and secondary Yb-RNA binding via bioinformatic approaches. We sought to computationally identify any shared structural motifs in the Yb-CLIP sequence tags but found no obvious motifs (data not shown).

***cis*-Regulatory Elements in *flam* and Other Genic piRNA Sources**

Genome-wide analysis of Yb-CLIP tags revealed that Yb binds various but particular regions across *flam* transcripts, and that the regions greatly overlap with *flam*-piRNA mapping regions (Figure 6A). Neither piRNAs nor Yb-CLIP tags were mapped on the neighboring gene, *Dip1* (Figure 6A). This further verifies a pivotal role for Yb in piRNA biogenesis substrate determination.

flam exons 1 and 2 are shared with *flam* isoforms in ovarian somatic sheet cells (equivalent to OSCs in this study) and fly ovaries (Goriaux et al., 2014). Both exons are also good targets for Yb binding (Figure 6A), so we examined if they act as *cis*-regulatory elements for piRNA production. For this, the *Tj-cis* element in the EGFP-*tj-cis* construct was replaced with either *flam* exon 1 or exon 2, yielding EGFP-*flam-e1* and EGFP-*flam-e2* (Figure 6B). Both exons produced artificial piRNAs from their downstream region (Figures 6C and S5A). We then fragmented exon 1 into R1 and R2 and repeated the assays. In accordance with Yb-CLIP results, R1 was predicted to bind Yb only weakly but it produced few artificial piRNAs. By contrast, R2, predicted to bind Yb relatively strongly, produced piRNAs similarly to

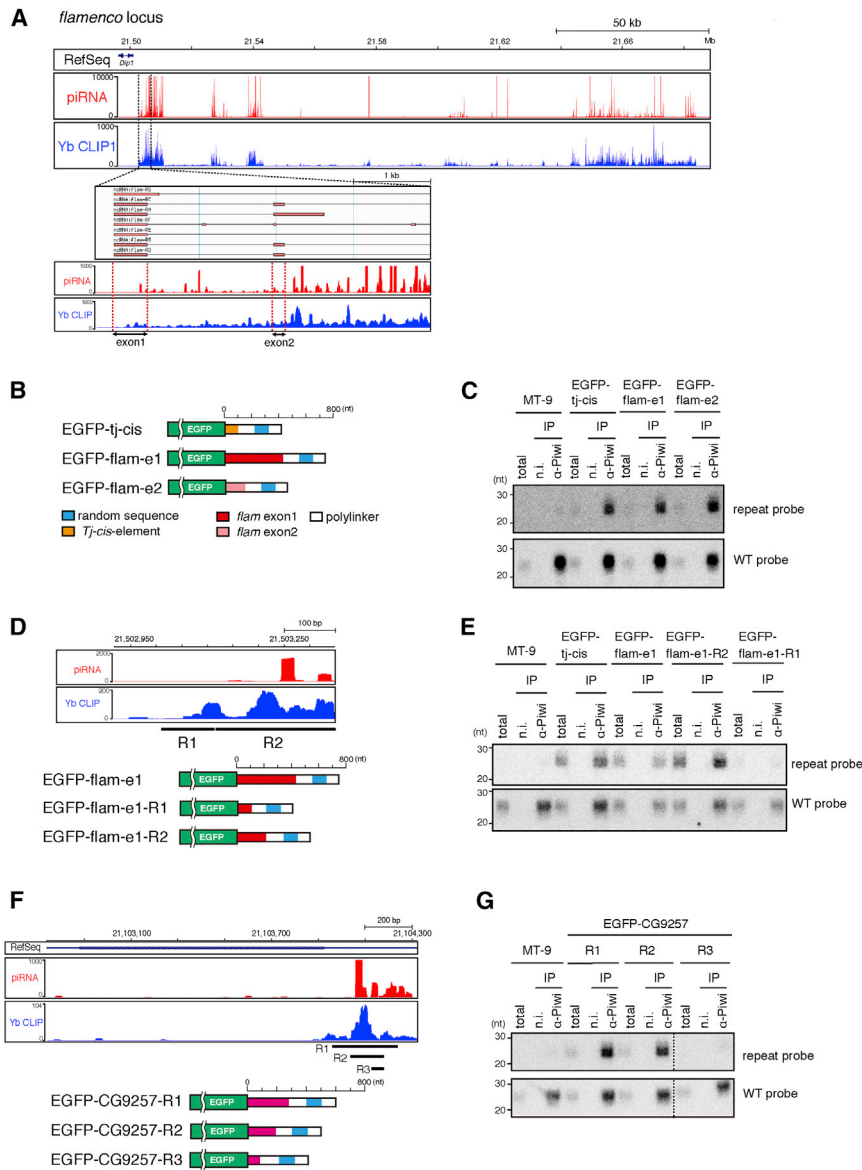


Figure 6. Analysis of *cis* Elements in *flam* and *CG9257* Transcripts

(A) A browser view of Yb-CLIP tags and piRNA sequences in wild-type OSCs (Figure 3C) mapped onto the *flam* locus. The bottom two rows show zoom-in mapping data of the top row. Signals are displayed as read counts.

(B) Schematic of EGFP-*tj-cis*, EGFP-*flam-e1*, and EGFP-*flam-e2*.

(C) Northern blotting was performed as in Figure 4B.

(D) A browser view of Yb-CLIP tags and piRNA sequences in wild-type OSCs (Figure 3C) mapped onto the *flam* exon 1. Two deletion mutants, R1 and R2, are indicated. Signals are displayed as read counts. Schematic of EGFP-*flam-e1*, EGFP-*flam-e1-R1*, and EGFP-*flam-e1-R2*.

(E) Northern blotting was performed as in Figure 4B.

(F) A browser view of Yb-CLIP tags and piRNA sequences in wild-type OSCs (Figure 3C) mapped onto the *CG9257* locus. Three fragments, R1, R2, and R3, used to produce the constructs are indicated. Signals are displayed as read counts. Schematic of EGFP-*CG9257-R1*, EGFP-*CG9257-R2*, and EGFP-*CG9257-R3* constructs.

(G) Northern blotting was performed as in Figure 4B.

full-length exon 1 (Figures 6D, 6E, and S5B). Yb-RNA binding therefore plays a crucial role in driving piRNA production.

We further extended our experiments to the genic piRNA gene *CG9257* (Saito et al., 2009). Yb-CLIP showed that Yb bound almost the entire 3' UTR of the transcripts (Figure 6F), and regions R1 and R2 in the *CG9257* 3' UTR acted as *cis*-regulatory elements similar to the *Tj-cis* element (Figures 6F and 6G). However, a deletion mutant of R2, R3, produced few piRNAs, despite its moderate binding with Yb. R3 may therefore represent a secondary binding site of Yb, as well as *Tj-R1* and *Tj-R2*.

Exogenously Expressed piRNAs Are Sufficiently Abundant to Elicit the Silencing of Endogenous Genes

Next, we assessed whether artificial piRNAs expressed under the control of the *Tj-cis* element were able to repress endoge-

nous genes in OSCs. We chose *Krimper* (*Krimp*) as an endogenous gene target because its knockdown previously had no effect on piRNA biogenesis or function (Olivieri et al., 2012). We constructed four plasmids (*Krimp-5'*, *Krimp-CDS-1*, *Krimp-CDS-2*, and *Krimp-3'*) expressing piRNAs targeting the 5' UTR, CDS-1 (1–50), CDS-2 (591–640), and the 3' UTR of *Krimp* mRNA, respectively (Figures 7A and 7B). All plasmids were based on the EGFP-*tj-cis* construct by inserting three identical copies of *Krimp* targeting sequences (50 nt each; except for the sequence targeting the 5' UTR, which was 72 nt) in front of the tandem repeats. The insertion was made in an antisense orientation; thus, piRNAs arising from the insertions should act as antisense to *Krimp* mRNAs. Northern blotting confirmed the expression of *Krimp*-piRNAs (Figure 7C).

To determine the efficiency of *Krimp*-piRNAs in *Krimp* silencing, OSCs were transfected with *Krimp-5'*, *Krimp-CDS-1*, *Krimp-CDS-2*, and *Krimp-3'*, together with another plasmid containing a blasticidin-resistance gene. On day 3 after transfection, blasticidin selection was applied to remove untransfected cells (Figure S6A). Western blotting with an anti-*Krimp* antibody (Nagao et al., 2011) showed that *Krimp* was significantly repressed in OSCs when *Krimp*-piRNAs targeting the *Krimp* CDS (1–50) and 3' UTR were expressed (Figure S6B). Conversely, *Krimp*-piRNAs targeting the 5' UTR and CDS (591–640) repressed *Krimp* to a lesser extent (Figure S6B).

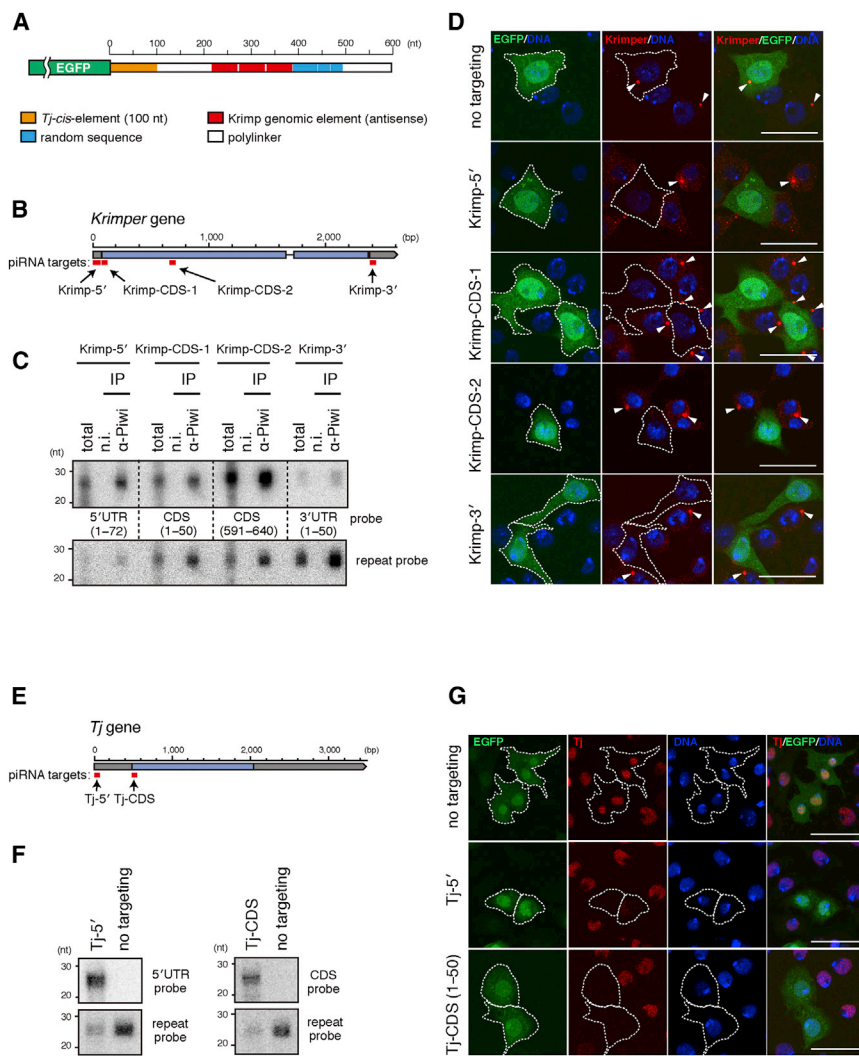


Figure 7. Artificial piRNAs Are Driven by the *Tj*-cis Element Silence Endogenous Genes in OSCs

(A) Schematic of constructs for expressing artificial *Krimp*-piRNAs. Genomic DNA fragments corresponding to *Krimp* 5' UTR, CDS-1, CDS-2, and the 3' UTR (see in B) are inserted three times into EGFP-*tj*-cis.

(B) Four regions in the *Krimp* gene were selected as *Krimp*-piRNA generation sites: *Krimp*-5' (1–72), *Krimp*-CDS-1 (1–50), *Krimp*-CDS-2 (591–640), and *Krimp*-3' (1–50).

(C) Production of exogenous *Krimp*-piRNAs was monitored by northern blotting. Artificial piRNAs expressed from the random sequence repeats (blue) were also detected.

(D) Immunofluorescence using anti-EGFP and anti-*Krimp* antibodies was performed on OSCs expressing exogenous *Krimp*-piRNAs. *Krimp* forms cytoplasmic foci called *Krimp* body (arrowheads), which are not observed in EGFP-positive OSCs. Scale bars represent 20 μ m.

(E) Two regions in the *Tj* gene were selected as *Tj*-piRNA generation sites: *Tj*-5' and *Tj*-CDS.

(F) The production of exogenous *Tj*-piRNAs was monitored by northern blotting using probes corresponding to the particular regions. Artificial piRNAs expressed from the random sequence repeats (blue) were also detected.

(G) Immunofluorescence using anti-EGFP and anti-*Tj* antibodies was performed on OSCs expressing exogenous *Tj*-piRNAs. Scale bars represent 20 μ m.

Considering that blasticidin treatment might not fully eliminate untransfected cells, leading to an apparent weakness in the silencing effect, we performed immunofluorescence using an anti-*Krimp* antibody. This determined the silencing effect only in cells in which *Krimp*-piRNAs had been generated, because cells considered EGFP-positive showed high EGFP mRNA expression, suggesting a high level of *Krimp*-piRNA expression. As expected, *Krimp* bodies (Nagao et al., 2011; Olivieri et al., 2012), cytoplasmic granules in which *Krimp* strongly accumulates, disappeared in EGFP-positive cells regardless of the constructs used for transfection (Figures 7D and S6C). This indicated that *Krimp* silencing occurred regardless of where *Krimp*-piRNAs targeted *Krimp* mRNA.

Krimp-piRNAs exogenously expressed from the constructs were loaded onto Piwi to form piRISCs (Figure 7C). To examine if *Krimp* silencing occurred Piwi-dependently, the efficiency of *Krimp* silencing was assessed in Piwi-depleted OSCs. When Piwi was present in OSCs, *Krimp* expression was strongly down-regulated by *Krimp*-piRNAs (Figure S6D). However, when Piwi was depleted, *Krimp* expression was restored (Figure S6D).

Thus, *Krimp* silencing mediated by exogenous piRNAs appears to be Piwi dependent. To assess whether *Krimp* silencing mediated by exogenous *Krimp*-piRNAs is transcriptional, we performed chromatin-immunoprecipitation (ChIP). The association of RNA pol II with *Krimp* was significantly reduced by *Krimp*-piRNAs targeting the *Krimp* CDS (1–50) and 3' UTR (Figure S6E). Under these conditions, the accumulation of H3K9me3 at *Krimp* increased (Figure S6E). The expression of *Krimp*-piRNAs in the sense orientation only slightly affected RNA pol II and H3K9me3 binding to *Krimp* (Figure S6F). These results suggest that exogenously expressed piRNAs trigger transcriptional silencing in OSCs.

We also set out to determine the silencing effect of artificial piRNAs against *Tj*. Primary piRNAs targeting *Tj* mRNAs (Figure 7E) were expressed in OSCs. Two plasmids were produced based on the EGFP-*tj*-cis construct, as in Figure 7A, by inserting three identical *Tj* targeting sequences (*Tj*-5' and *Tj*-CDS; 50 nt each) in front of the tandem repeats. Northern blotting confirmed the expression of corresponding piRNAs (Figure 7F). Immunofluorescence using anti-*Tj* antibodies showed that EGFP-positive cells expressing artificial *Tj*-5'-piRNAs and *Tj*-CDS-piRNAs lacked *Tj* signals in the nucleus (Figure 7G) (note that these artificial piRNAs were “antisense” to *Tj* mRNA while endogenous

Tj-piRNAs are “sense” to *Tj* mRNA). Thus, artificial piRNAs produced under control of the *Tj-cis* element appear capable of silencing endogenous genes.

DISCUSSION

Yb bodies and Flam bodies in OSCs are considered to be the centers for primary piRNA maturation/piRISC formation and piRNA intermediate storage, respectively, and exist in close proximity (Murota et al., 2014; Olivieri et al., 2010; Saito et al., 2010). The formation of both bodies depends on the Yb protein, particularly its RNA-binding activity (Murota et al., 2014). In the absence of this, piRNA processing fails, resulting in piRNA loss, although piRNA intermediates and processing factors are present in the cytosol. Thus, Yb binding to piRNA sources centralizes all necessary ingredients for piRNA biogenesis, which is crucial for primary piRNA production (Murota et al., 2014). In this study, we continued the study on Yb and discovered that the direct association of Yb with a specific ~100-nt element (i.e., *cis* element) within the piRNA precursors provokes somatic primary piRNA biogenesis from downstream regions. Insertion of the Yb-binding element within RNA molecules that do not otherwise serve as piRNA precursors converts the RNA transcripts into piRNA sources. Artificial primary piRNAs were mapped only downstream, but not upstream, of regions of the Yb-binding element. Previous studies demonstrated that natural genic piRNAs mostly arise from 3' UTRs rather than mRNA CDS or 5' UTRs (Robine et al., 2009; Saito et al., 2009). The present study also showed that few *Tj*-piRNAs mapped to the *Tj* CDS (Figure 3C), and that few Yb-CLIP tags were also found in the *Tj* CDS (Figure 5A). Thus, Yb determines not only substrate specificity but also processing directionality in the somatic primary piRNA biogenesis pathway. This may occur through the Yb-controlled recruitment of other piRNA factors, such as another putative RNA helicase *Armi* and endonuclease *Zuc*, only to downstream sequences. We are currently investigating this possibility.

Yb-CLIP tags greatly overlap with primary piRNA-producing loci in the genome. This strongly supports the idea that Yb is the central player in determining substrates in the piRNA pathway. An unexpected but intriguing observation in our study is that *Tj-R1* and *Tj-R2* in the *Tj* 3' UTR show strong Yb-binding marks, as does the *Tj-cis* element, but provoked very little artificial piRNA production in contrast to the *Tj-cis* element (Figure 5B). Yb-CLIP experiments showed that Yb binding to *Tj-R1* and *Tj-R2* within the *Drosophila* genome largely depends on Yb binding to its upstream *Tj-cis* element (Figure 5D). We therefore propose a model in which Yb determines primary piRNA sources by two sequential modes of action: primary binding to *cis* elements that represents selection of piRNA precursors among cellular RNAs, then secondary binding to downstream regions, representing the defining domains to be processed by precursors (Figure S7). This complexity in determining piRNA precursors could ensure the high diversity in piRNA populations, which is a unique feature of piRNAs (Aravin et al., 2007; Brennecke et al., 2007; Lau et al., 2009).

The RNA-binding activity of Yb is required for primary piRNA production in OSC. Yb mutants carrying a point mutation within

the DEAD box showed little RNA binding activity (Murota et al., 2014). When these Yb mutants were expressed individually in OSC lacking endogenous Yb, piRNA precursors were not accumulated in Flam bodies, and few piRNAs were produced. As a consequence, transposons were de-silenced. Therefore, there is little doubt that the RNA-binding activity of Yb through the DEAD-box is indispensable for primary piRNA production. HITS-CLIP experiments clarified direct interaction of Yb with piRNA sources, including *Tj* mRNA. Insertion of a particular Yb-bound RNA element within *Tj* mRNA, i.e., the *Tj-cis* element, upstream of any given RNA molecule enables the arbitrary sequences to produce artificial piRNAs. Deletion of the *Tj-cis* element from the *Drosophila* genome significantly abolished piRNA production from its downstream region spanning at least ~200 nt. These observations strongly support our model (Figure S7), in which Yb is the *trans*-acting factor that recognizes and binds *cis* elements within piRNA precursors to provoke primary piRNA biogenesis in ovarian somatic cells. However, it does not exclude the possibility that Yb collaboratively achieves this task with unknown factors. Moreover, we are not certain if Yb is the uppermost factor in the cytoplasmic phase of the biogenesis pathway upon nuclear transport of piRNA precursors. We are currently engaged in addressing these challenging questions in the laboratory.

EXPERIMENTAL PROCEDURES

Cell Culture and Transfection

OSCs were cultured as described previously (Saito et al., 2009; Niki et al., 2006). OSC transfection was carried out using Xfect Transfection Reagent (Clontech) as described previously (Murota et al., 2014). Blasticidin (Life Technologies) was added to the media at 50 µg/ml upon co-transfection using a plasmid carrying a blasticidin-resistant gene. RNAi was performed as described previously (Murota et al., 2014).

Plasmid Construction

To generate the EGFP-*tj* WT construct, the full-length *Tj* 3' UTR was first PCR-amplified with the primers *tj*-3'UTR F/R (Table S1, all oligonucleotides were purchased from Invitrogen) from OSC cDNA samples using KOD plus DNA polymerase (Toyobo) and then cloned between XhoI and BamHI sites of pEGFP-C1 (Clontech). The polylinker region between EGFP and *Tj* 3' UTR was removed by inverse PCR using the primers *delta-mcs* F/R. The EGFP-*tj* 3' UTR insert was subcloned into the NheI and BamHI sites of pAcM (Saito et al., 2009). The Cas9 plasmid, p_{hsp70}-Cas9, and the sgRNA plasmid, pU6-BbsI-chiRNA, were purchased from Addgene. Target sequences were synthesized as oligomers and inserted into the BbsI site of pU6-BbsI-chiRNA. Detailed methods for constructing other plasmids are described in the Supplemental Information.

Derivation of the *Tj-cis* Element Deletion Mutant OSCs

OSCs were transfected with 4 µg of Cas9 plasmid, 4 µg of sgRNA plasmids, and 400 ng of the blasticidin resistance gene plasmid as described above. Cells were incubated for 48 hr post-transfection prior to blasticidin selection. Three days after addition of blasticidin, 5.0×10^3 cells were passaged in 6-cm dishes and allowed to grow in blasticidin containing medium. After 6–7 days of culture, colonies were picked and passaged in single wells of 24-well plates and allowed to grow to confluence in blasticidin free medium. Genomic DNA was extracted using QuickExtract DNA Extraction Solution (Epicenter) following the manufacturer's protocol. The genomic region flanking the CRISPR target site was PCR amplified and analyzed by electrophoresis on 1% agarose gels.

Immunoprecipitation

Immunoprecipitation from OSCs was performed as previously described (Saito et al., 2009). Anti-Piwi antibody (Saito et al., 2006) was immobilized on

Dynabeads protein G (Invitrogen). Total RNAs were isolated from the immunoprecipitates with phenol-chloroform and precipitated with ethanol.

Northern Blotting

Total RNA was isolated from OSCs using RNAzol RT (Molecular Research Center). Any contaminating DNA was digested by TURBO DNase (Ambion). For small RNA detection, northern blotting analysis was carried out using 5 µg of total RNAs as described previously (Saito et al., 2006). The DNA oligonucleotides used are summarized in Table S1. mRNAs were purified from 20 µg of total RNA using Oligotex-dT30 (Takara) according to the manufacturer's instructions, and northern blotting analysis was carried out as described previously (Murota et al., 2014). DNA probes were synthesized using a Random Primer DNA Labeling Kit Ver. 2 (Takara) in the presence of ³²P-dCTP. Templates of random-primed probes were generated by PCR. For the EGFP probe, the EGFP ORF was amplified using the primers EGFP F/R with EGFP-C1 vector as template. For the GAPDH probe, the GAPDH ORF was amplified using the primers GAPDH F/R with OSC cDNA as template.

Western Blotting

Western blotting was performed as described previously (Saito et al., 2006). Anti-Piwi (Saito et al., 2006) (1:1,000 dilution), anti-EGFP (MBL) (1:1,000 dilution), anti-Yb (Murota et al., 2014) (1:1,000 dilution), and anti-tubulin (DSHB) (1:2,000 dilution) antibodies were used.

Small RNA Cloning and Sequencing

For piRNA cloning, coimmunoprecipitated piRNA was extracted from Piwi immunoprecipitates using phenol and chloroform, and gel-purified piRNAs were cloned using the NEBNext Small RNA Library Sample Prep Set (NEB). piRNA libraries were analyzed on a HiSeq2000 (Illumina).

Small RNA Sequencing Data Analysis

Sequencing of small RNA libraries generated from Piwi immunoprecipitates were performed using HiSeq2000. Adaptor sequences were removed from obtained reads and mapped to the Release 5 assembly of the *Drosophila* genome using Bowtie (Langmead et al., 2009), allowing zero mismatch and extracting the reads mapped uniquely to the genome. Reads originating from EGFP-tj-cis construct were mapped against construct sequence using Bowtie, allowing zero mismatch and default parameters. The reads were normalized to RPM (read per million) by the number of *Drosophila* genome-mapped reads.

HITS-CLIP

CLIP was performed basically as described previously (Jaskiewicz et al., 2012). OSCs (1–2 × 10⁸) were UV crosslinked by irradiating uncovered with 200 mJ/cm² of 254 nm UV, followed by lysis with lysis buffer (20 mM HEPES-KOH [pH 7.3], 1 mM EDTA, 1 mM DTT, 150 mM sodium chloride, 2 µg/ml pepstatin, 2 µg/ml leupeptin, 0.5% aprotinin, 0.5% NP40), and cell debris was removed by centrifugation. Immunoprecipitation was performed using 20 µg of anti-Yb antibody (Murota et al., 2014), followed by the treatment of 10 U/µl RNaseT1 (Roche). Dephosphorylation of RNA segments crosslinked to immunoprecipitated proteins was performed by calf intestinal alkaline phosphatase (CIP form NEB), and the samples were 5' end labeled, followed by NuPAGE (Life Technologies) and transfer to the membrane. Protein-bound RNA signal was cut out from the membrane, and RNA was isolated by phenol/chloroform extraction. For library construction, preadenylated 3' adaptor was ligated to the RNA samples using T4 RNA Ligase 2, truncated KQ (NEB), followed by 5' adaptor ligation using T4 RNA Ligase 1 (NEB). Adaptor-ligated RNA samples were reverse transcribed using SuperScript III (Life Technologies) and PCR amplified using Q5 High-Fidelity DNA Polymerase (NEB).

Bioinformatic Analysis

CLIP tags were mapped to Release 5 assembly of the *Drosophila* genome as previously described (Murota et al., 2014). CIMSs were detected according to Zhang and Darnell (2011). For each genomic position where at least one deletion was observed on the mapped CLIP tags, the number of mapped CLIP tags (*k*) and that of tags with deletions (*m*) were counted. The null distribution of *m* for given *k* was obtained by permuting positions of the deletions. The permutation was conducted by preserving the distribution of the CLIP tags on the

genome and the positional distribution of deletions relative to the 5' ends of the CLIP tags. The false discovery rate (FDR) was estimated using the cumulative distributions of *m* for a given *k*, and the positions with FDR <0.01 were detected as CIMSs.

Assessing Reproducibility of HITS-CLIP Data

Given two biological replicate data sets of HITS-CLIP, their reproducibility was assessed as follows. For each CIMS, in one data set (*query*) and in the other (*target*), we collected reads that were mapped to the CIMS position and to the same strand using BEDTools (version 2.18.1) and an in-house Perl script. The boundaries of each read *cluster* were defined as the left-most and right-most positions of the collected reads. For each cluster in *query*, the cluster in *target* that overlapped with it by at least 1 bp and whose CIMS position was closest to the *query* CIMS position was identified. Then, Pearson and Spearman's rank correlation coefficients between their read numbers were calculated. If multiple clusters in *target* satisfied the above criterion (i.e., with the same CIMS distances), the averaged read number was used.

RIP and qPCR

OSCs (4–5 × 10⁷) were homogenized in lysis buffer (20 mM HEPES-KOH [pH 7.3], 150 mM sodium chloride, 1 mM DTT, 1 mM EDTA, 2 µg/ml pepstatin, 2 µg/ml leupeptin, 0.5% aprotinin, 0.5% NP40, and 40 U/ml RNasin [Promega]), and cell debris was removed by centrifugation. One-tenth of the lysate was saved as RNA input, and total RNAs were isolated using ISOGEN-LS reagent (Nippongene). Anti-Yb antibody (Murota et al., 2014) (2 µg) was immobilized on Dynabeads protein G. Lysates were incubated with beads for 2 hr at 4°C before washing three times with IP wash buffer (20 mM HEPES-KOH [pH 7.3], 300 mM sodium chloride, 1 mM DTT, 2 µg/ml pepstatin, 2 µg/ml leupeptin, 0.5% aprotinin, 0.05% NP40) and three times with high-salt wash buffer (20 mM HEPES-KOH [pH 7.3], 500 mM sodium chloride, 1 mM DTT, 2 µg/ml pepstatin, 2 µg/ml leupeptin, 0.5% aprotinin, and 0.05% NP40). Total RNAs were isolated from the immunoprecipitates with phenol-chloroform and were precipitated with ethanol. For qPCR analysis following RNA immunoprecipitation, a fixed volume of RNA isolated from input and immunoprecipitates was used for reverse transcription. Reverse transcription was performed using ReverTra Ace qPCR RT Master Mix (Toyobo). qPCRs were performed using the specific qPCR primers mcs F/R (Table S1) in the StepOnePlus Real-Time PCR System (Life Technologies). THUNDERBIRD SYBR qPCR Mix (Toyobo) was used as described in the instruction manual. The specific enrichment was analyzed based on a percent input calculation.

Immunofluorescence

Immunofluorescence of OSCs was performed using anti-EGFP IgG2b (MBL) (1:500 dilution), anti-Krimp IgG1 (Nagao et al., 2011) (1:250 dilution), and anti-TJ IgG1 (1:250 dilution) antibodies as described previously (Murota et al., 2014). Alexa-Fluor-488-conjugated anti-mouse IgG2b (Molecular Probes) and Alexa-Fluor-594-conjugated anti-mouse IgG1 (Molecular Probes) antibodies were used as secondary antibodies (1:1,000 dilution). Anti-TJ monoclonal antibody was produced by immunizing mice with GST-TJ protein as previously described (Saito et al., 2009).

ChIP and qPCR

OSCs (1–2 × 10⁸) were crosslinked with 1% formaldehyde for 5 min at room temperature, and crosslinking was then quenched with 125 mM glycine for 5 min at room temperature. Fixed cells were washed twice with PBS, harvested by scraping, lysed with swelling buffer (25 mM HEPES-KOH [pH 7.3], 1.5 mM magnesium chloride, 10 mM potassium chloride, 0.1% NP40, 1 mM DTT, 1 × Halt Protease Inhibitor Cocktail [Thermo Scientific]), and pelleted. Nuclear pellets were extracted by sonication buffer (50 mM HEPES-KOH [pH 7.3], 140 mM sodium chloride, 1 mM EDTA, 1% Triton X-100, 0.1% sodium deoxycholate, 0.1% SDS, 1 × Halt Protease Inhibitor Cocktail), sonicated in a Covaris S220 focused ultrasonicator, and diluted. After removing input, the DNA-protein complexes were incubated with 2 µg of nonimmune IgG antibody, anti-Pol II antibody 4H8 (CST), or anti-H3K9me3 antibody (Active motif) at 4°C overnight. DNA-protein complexes were precipitated using Dynabeads Protein G for 1 hr. The beads were consequently washed with low-salt wash buffer (20 mM Tris-HCl [pH 8.0], 150 mM sodium chloride, 2 mM EDTA,

0.1% SDS, 0.1% Triton X-100, 1 mM PMSF), high-salt wash buffer (20 mM Tris-HCl [pH 8.0], 500 mM sodium chloride, 2 mM EDTA, 0.1% SDS, 0.1% Triton X-100, 1 mM PMSF), LiCl wash buffer (10 mM Tris-HCl [pH 8.0], 1 mM EDTA, 250 mM lithium chloride, 1% NP40, 1% sodium deoxycholate, 1 mM PMSF), and twice with TE (10 mM Tris-HCl [pH 8.0], 1 mM EDTA, 1 mM PMSF). After washing, immunoprecipitated chromatin was eluted by elution buffer (50 mM Tris-HCl [pH 8.0], 10 mM EDTA, 1% SDS). Eluted chromatin and input samples were reverse crosslinked for 12–16 hr at 65°C. ChIP DNA was treated with RNase A for 30 min at 37°C, and then treated with proteinase K for 60 min at 55°C. DNA was purified by extraction with phenol/chloroform/isoamyl alcohol and ethanol precipitation. Pellet Paint NF Co-Precipitant (Merck Millipore) was added to the DNA prior to precipitation. qPCRs were performed using ChIP DNA with specific qPCR primers Krimper F/R (Table S1) in StepOnePlus Real-Time PCR Systems. THUNDERBIRD SYBR qPCR Mix was used as described in the instruction manual. The specific enrichment was analyzed by percentage input calculation.

ACCESSION NUMBERS

Deep sequencing data sets have been deposited in the NCBI GEO and are available under accession number GEO: GSE69625.

SUPPLEMENTAL INFORMATION

Supplemental Information includes Supplemental Experimental Procedures, seven figures, and one table and can be found with this article online at <http://dx.doi.org/10.1016/j.celrep.2015.06.035>.

ACKNOWLEDGMENTS

We thank the other members of the M.C.S. laboratories for their discussions and comments on the manuscript. We also thank T. Fukunaga for bioinformatics assistance. This work was supported by a Grant-in-Aid for Scientific Research from the Ministry of Education, Culture, Sports, Science and Technology (MEXT) of Japan to H.I., Y.W.I., W.I., H.S., and M.C.S.

Received: May 19, 2015

Revised: June 8, 2015

Accepted: June 10, 2015

Published: July 9, 2015

REFERENCES

- Aravin, A.A., Hannon, G.J., and Brennecke, J. (2007). The Piwi-piRNA pathway provides an adaptive defense in the transposon arms race. *Science* *318*, 761–764.
- Brennecke, J., Aravin, A.A., Stark, A., Dus, M., Kellis, M., Sachidanandam, R., and Hannon, G.J. (2007). Discrete small RNA-generating loci as master regulators of transposon activity in *Drosophila*. *Cell* *128*, 1089–1103.
- Choi, S.Y., Huang, P., Jenkins, G.M., Chan, D.C., Schiller, J., and Frohman, M.A. (2006). A common lipid links Mfn-mediated mitochondrial fusion and SNARE-regulated exocytosis. *Nat. Cell Biol.* *8*, 1255–1262.
- Dönertas, D., Sienski, G., and Brennecke, J. (2013). *Drosophila* Gtsf1 is an essential component of the Piwi-mediated transcriptional silencing complex. *Genes Dev.* *27*, 1693–1705.
- Ghildiyal, M., and Zamore, P.D. (2009). Small silencing RNAs: an expanding universe. *Nat. Rev. Genet.* *10*, 94–108.
- Goriaux, C., Desset, S., Renaud, Y., Vaury, C., and Brasset, E. (2014). Transcriptional properties and splicing of the *flamenco* piRNA cluster. *EMBO Rep.* *15*, 411–418.
- Haase, A.D., Fenoglio, S., Muerdter, F., Guzzardo, P.M., Czech, B., Pappin, D.J., Chen, C., Gordon, A., and Hannon, G.J. (2010). Probing the initiation and effector phases of the somatic piRNA pathway in *Drosophila*. *Genes Dev.* *24*, 2499–2504.
- Han, B.W., Wang, W., Li, C., Weng, Z., and Zamore, P.D. (2015). Noncoding RNA. piRNA-guided transposon cleavage initiates Zucchini-dependent, phased piRNA production. *Science* *348*, 817–821.
- Houwing, S., Kamminga, L.M., Berezikov, E., Cronembold, D., Girard, A., van den Elst, H., Filippov, D.V., Blaser, H., Raz, E., Moens, C.B., et al. (2007). A role for Piwi and piRNAs in germ cell maintenance and transposon silencing in Zebrafish. *Cell* *129*, 69–82.
- Hsu, P.D., Lander, E.S., and Zhang, F. (2014). Development and applications of CRISPR-Cas9 for genome engineering. *Cell* *157*, 1262–1278.
- Huang, X.A., Yin, H., Sweeney, S., Raha, D., Snyder, M., and Lin, H. (2013). A major epigenetic programming mechanism guided by piRNAs. *Dev. Cell* *24*, 502–516.
- Ipsaro, J.J., Haase, A.D., Knott, S.R., Joshua-Tor, L., and Hannon, G.J. (2012). The structural biochemistry of Zucchini implicates it as a nuclease in piRNA biogenesis. *Nature* *491*, 279–283.
- Ishizu, H., Siomi, H., and Siomi, M.C. (2012). Biology of PIWI-interacting RNAs: new insights into biogenesis and function inside and outside of germlines. *Genes Dev.* *26*, 2361–2373.
- Jaskiewicz, L., Bilien, B., Hausser, J., and Zavolan, M. (2012). Argonaute CLIP—a method to identify *in vivo* targets of miRNAs. *Methods* *58*, 106–112.
- Juliano, C., Wang, J., and Lin, H. (2011). Uniting germline and stem cells: the function of Piwi proteins and the piRNA pathway in diverse organisms. *Annu. Rev. Genet.* *45*, 447–469.
- Kawaoka, S., Hayashi, N., Suzuki, Y., Abe, H., Sugano, S., Tomari, Y., Shimada, T., and Katsuma, S. (2009). The *Bombyx* ovary-derived cell line endogenously expresses PIWI/PIWI-interacting RNA complexes. *RNA* *15*, 1258–1264.
- Khurana, J.S., and Theurkauf, W. (2010). piRNAs, transposon silencing, and *Drosophila* germline development. *J. Cell Biol.* *191*, 905–913.
- Langmead, B., Trapnell, C., Pop, M., and Salzberg, S.L. (2009). Ultrafast and memory-efficient alignment of short DNA sequences to the human genome. *Genome Biol.* *10*, R25.
- Lau, N.C., Robine, N., Martin, R., Chung, W.J., Niki, Y., Berezikov, E., and Lai, E.C. (2009). Abundant primary piRNAs, endo-siRNAs, and microRNAs in a *Drosophila* ovary cell line. *Genome Res.* *19*, 1776–1785.
- Li, M.A., Alls, J.D., Avancini, R.M., Koo, K., and Godt, D. (2003). The large Maf factor Traffic Jam controls gonad morphogenesis in *Drosophila*. *Nat. Cell Biol.* *5*, 994–1000.
- Malone, C.D., Brennecke, J., Dus, M., Stark, A., McCombie, W.R., Sachidanandam, R., and Hannon, G.J. (2009). Specialized piRNA pathways act in germline and somatic tissues of the *Drosophila* ovary. *Cell* *137*, 522–535.
- Mohn, F., Handler, D., and Brennecke, J. (2015). Noncoding RNA. piRNA-guided slicing specifies transcripts for Zucchini-dependent, phased piRNA biogenesis. *Science* *348*, 812–817.
- Muerdter, F., Guzzardo, P.M., Gillis, J., Luo, Y., Yu, Y., Chen, C., Fekete, R., and Hannon, G.J. (2013). A genome-wide RNAi screen draws a genetic framework for transposon control and primary piRNA biogenesis in *Drosophila*. *Mol. Cell* *50*, 736–748.
- Murota, Y., Ishizu, H., Nakagawa, S., Iwasaki, Y.W., Shibata, S., Kamatani, M.K., Saito, K., Okano, H., Siomi, H., and Siomi, M.C. (2014). Yb integrates piRNA intermediates and processing factors into perinuclear bodies to enhance piRISC assembly. *Cell Rep.* *8*, 103–113.
- Nagao, A., Sato, K., Nishida, K.M., Siomi, H., and Siomi, M.C. (2011). Gender-specific hierarchy in nuage localization of PIWI-interacting RNA factors in *Drosophila*. *Front. Genet.* *2*, 55.
- Niki, Y., Yamaguchi, T., and Mahowald, A.P. (2006). Establishment of stable cell lines of *Drosophila* germ-line stem cells. *Proc. Natl. Acad. Sci. USA* *103*, 16325–16330.
- Nishimasu, H., Ishizu, H., Saito, K., Fukuhara, S., Kamatani, M.K., Bonnefond, L., Matsumoto, N., Nishizawa, T., Nakanaga, K., Aoki, J., et al. (2012). Structure and function of Zucchini endoribonuclease in piRNA biogenesis. *Nature* *491*, 284–287.

- Ohtani, H., Iwasaki, Y.W., Shibuya, A., Siomi, H., Siomi, M.C., and Saito, K. (2013). DmGTSF1 is necessary for Piwi-piRISC-mediated transcriptional transposon silencing in the *Drosophila* ovary. *Genes Dev.* *27*, 1656–1661.
- Olivieri, D., Sykora, M.M., Sachidanandam, R., Mechtler, K., and Brennecke, J. (2010). An *in vivo* RNAi assay identifies major genetic and cellular requirements for primary piRNA biogenesis in *Drosophila*. *EMBO J.* *29*, 3301–3317.
- Olivieri, D., Senti, K.A., Subramanian, S., Sachidanandam, R., and Brennecke, J. (2012). The cochaperone shutdown defines a group of biogenesis factors essential for all piRNA populations in *Drosophila*. *Mol. Cell* *47*, 954–969.
- Qi, H., Watanabe, T., Ku, H.Y., Liu, N., Zhong, M., and Lin, H. (2011). The Yb body, a major site for Piwi-associated RNA biogenesis and a gateway for Piwi expression and transport to the nucleus in somatic cells. *J. Biol. Chem.* *286*, 3789–3797.
- Robine, N., Lau, N.C., Balla, S., Jin, Z., Okamura, K., Kuramochi-Miyagawa, S., Blower, M.D., and Lai, E.C. (2009). A broadly conserved pathway generates 3'UTR-directed primary piRNAs. *Curr. Biol.* *19*, 2066–2076.
- Saito, K., Nishida, K.M., Mori, T., Kawamura, Y., Miyoshi, K., Nagami, T., Siomi, H., and Siomi, M.C. (2006). Specific association of Piwi with rasiRNAs derived from retrotransposon and heterochromatic regions in the *Drosophila* genome. *Genes Dev.* *20*, 2214–2222.
- Saito, K., Inagaki, S., Mituyama, T., Kawamura, Y., Ono, Y., Sakota, E., Kotani, H., Asai, K., Siomi, H., and Siomi, M.C. (2009). A regulatory circuit for *piwi* by the large Maf gene *traffic jam* in *Drosophila*. *Nature* *461*, 1296–1299.
- Saito, K., Ishizu, H., Komai, M., Kotani, H., Kawamura, Y., Nishida, K.M., Siomi, H., and Siomi, M.C. (2010). Roles for the Yb body components Armitage and Yb in primary piRNA biogenesis in *Drosophila*. *Genes Dev.* *24*, 2493–2498.
- Siomi, M.C., Sato, K., Pezic, D., and Aravin, A.A. (2011). PIWI-interacting small RNAs: the vanguard of genome defence. *Nat. Rev. Mol. Cell Biol.* *12*, 246–258.
- Sugimoto, Y., König, J., Hussain, S., Zupan, B., Curk, T., Frye, M., and Ule, J. (2012). Analysis of CLIP and iCLIP methods for nucleotide-resolution studies of protein-RNA interactions. *Genome Biol.* *13*, R67.
- Szakmary, A., Reedy, M., Qi, H., and Lin, H. (2009). The Yb protein defines a novel organelle and regulates male germline stem cell self-renewal in *Drosophila melanogaster*. *J. Cell Biol.* *185*, 613–627.
- Vagin, V.V., Sigova, A., Li, C., Seitz, H., Gvozdev, V., and Zamore, P.D. (2006). A distinct small RNA pathway silences selfish genetic elements in the germline. *Science* *313*, 320–324.
- Zamparini, A.L., Davis, M.Y., Malone, C.D., Vieira, E., Zavadil, J., Sachidanandam, R., Hannon, G.J., and Lehmann, R. (2011). Vreteno, a gonad-specific protein, is essential for germline development and primary piRNA biogenesis in *Drosophila*. *Development* *138*, 4039–4050.
- Zhang, C., and Darnell, R.B. (2011). Mapping *in vivo* protein-RNA interactions at single-nucleotide resolution from HITS-CLIP data. *Nat. Biotechnol.* *29*, 607–614.